

# Strange particles in dense matter and kaon condensates

G.E. Brown, C.-H. Lee, and R. Rapp<sup>a \*</sup>

<sup>a</sup>Department of Physics, State University of New York at Stony Brook, Stony Brook, NY 11794-3800, USA

We discuss the role of strangeness in dense matter and especially in neutron stars. The early (in density) introduction of hyperons found in many calculations is probably delayed by the decrease in vector mean field acting on the neutron. This decrease results from both conventional many-body rescattering effects and from the movement towards asymptotic freedom at high densities. Subthreshold  $K^-$ -meson production by the KaoS collaboration at GSI shows that the  $K^-$ -mass must be substantially lowered, by  $\geq 200$  MeV at  $\rho \sim 2\rho_0$ . It is shown that explicit chiral symmetry breaking through the kaon mass may be responsible for  $\Sigma^-$ -nucleon and  $\Xi^-$ -nucleon scalar attraction being weaker than obtained by simple quark scaling. The normal mode of the strangeness minus, charge  $e^-$ , excitation is constructed as a linear combination of  $K^-$ -meson and  $\Sigma^-$ , neutron-hole state. Except for zero momentum, where the terms are unmixed, the “kaesobar” is a linear combination of these two components.

## 1. INTRODUCTION

Strangeness has been introduced into dense matter, at supranuclear densities, in many ways. Most simply, strange quarks have been included in quark seas making up the neutron star. This seems energetically favorable, since introducing strange quarks can relieve the high Fermi energies of the nonstrange quarks [1,2]. Bethe, Brown and Cooperstein [3] pointed out that such efforts gave a transition from hadrons to quarks at much too low a density, because confining forces were left out in the quark sector. Although we now believe that chiral restoration in the up and down quarks takes place at  $\rho \leq 3\rho_0$  [4], the strange quark condensate exists until substantially higher densities, so it is more appropriate to use the hadron language for strange hadrons at densities  $\rho \sim 3\rho_0$  which we discuss here.

Breaking of strangeness takes only a fraction of a second, so that in astrophysics there is sufficient of time for it except in the initial bounce of a collapsing star, where dynamical times are  $\sim 1$  millisecond. Following the bounce the compact core of a large star goes through a period of Kelvin-Helmholtz contraction, heating up as the trapped neutrinos in the interior diffuse out of the core, leaving most of the energy in the core as heat. In the

---

\*Supported by the U.S. Department of Energy under grant no. DE-FG02-88ER40388. We would like to thank Avraham Gal for useful criticism and advice. One of us (RR) acknowledges support from the Alexander-von-Humboldt foundation as a Feodor-Lynen fellow.

few seconds in which enough of the trapped neutrinos leave, so that the phase transitions we discuss below can take place, the temperature increases to  $T \sim 50$  MeV.

The strange particles  $K^-$ ,  $\Sigma^-$  and  $\Xi^-$  carry negative charge. Thus, as the chemical potential  $\mu_{e^-}$  goes up with increasing density, it becomes favorable to replace electrons by strange particles, really the negative charge being the important quantity.

Given linear, in density, extrapolation from nuclear matter density, it is clear that  $\Sigma^-$  baryons will quickly come in. In fact,  $\Lambda$ 's generally enter first, but since they carry no charge, they effectively change only little the behavior of the predominantly neutron star. The  $\Sigma^-$  can replace both neutron and electron. It comes in at the density  $\rho_c$  where

$$\mu_{\Sigma^-} = \mu_n + \mu_{e^-}. \quad (1)$$

In this case a  $\Sigma^-$  at rest replaces a neutron at the top of its Fermi sea, with Fermi momentum  $k_{F_n} \sim 500$  MeV for  $\rho \sim 3\rho_0$  and an electron. It proves convenient to regard the  $\Sigma^-$ -particle, neutron-hole as an excitation, as shown in Figure 1

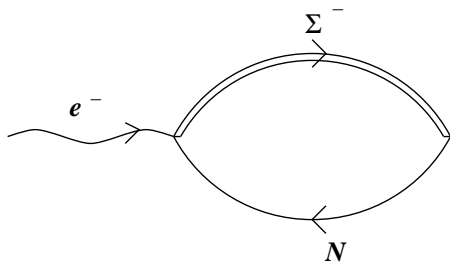


Figure 1. The  $\Sigma^- N^{-1}$  excitation can replace an electron in a neutron star once the condition of Eq. (1) is met.

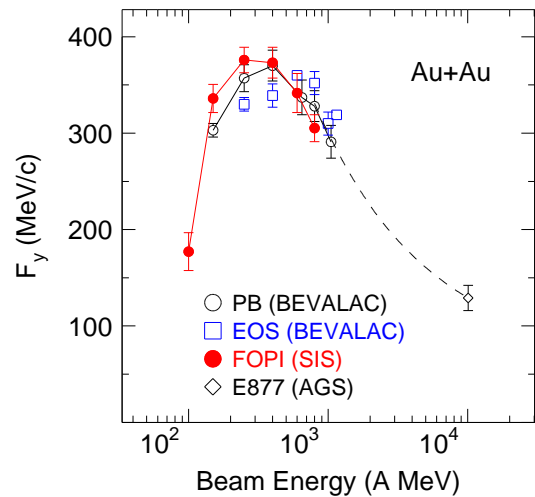


Figure 2. The sideways flow as measured in Au+Au heavy ion collisions [11].

Nowadays nobody makes the naive extrapolation in density we now outline, but in a schematic way it represents the chief features of what goes on. With  $k_{F_n} \sim 500$  MeV (at  $\rho \sim 3\rho_0$ ) and with chiral restoration at a density  $\rho \leq 3\rho_0$ , all of the nucleon mass here comes from the explicit chiral symmetry breaking through the low quark masses [5]  $m_n^* \sim 200 - 300$  MeV, the neutron energy at the top of its Fermi sea is

$$E_{F_n} \simeq \mu_n \geq 500 \text{ MeV} + V \quad (2)$$

where  $V$  is the vector potential felt by the neutron. For  $\rho \sim \rho_0$ ,  $V \simeq 275$  MeV in the linear Walecka model [6]. Thus, with a linear extrapolation to  $\rho = 3\rho_0$ ,  $\mu_n \geq 1325$  MeV.

From this it is clear that the condition Eq. (1) is met at a density  $< 3\rho_0$ , generally for  $\rho \sim 2\rho_0$ , even in more complete theories.

Two points have been made clear by our model:

1. The  $\Sigma^- N^{-1}$  excitation has a high momentum,  $k \sim 500$  MeV at  $\rho \sim 3\rho_0$ .
2. It's predominantly the vector mean field which pushes the neutron energy up towards  $M_{\Sigma^-}$  (and beyond in our schematic model).

Now, two agencies operate so as to reduce the vector mean field at high densities, one simple and well understood, the other somewhat tentative and not yet well understood.

Firstly, rescattering corrections reduce a highly repulsive interaction in many-body theory, essentially through screening. Thus, the Dirac-Brueckner-Hartree-Fock calculation [7], although consistent with the Walecka model for  $\rho = \rho_0$ , reduces the vector mean field by a factor  $\sim 0.6$  for  $\rho \sim 3\rho_0$ . As can immediately be seen, this moves the possible participation of  $\Sigma^-$ -hyperons from  $\rho \sim 2\rho_0$  to  $\rho \sim 3\rho_0$ , and this is why we discuss this latter density.

The second point has to do with chiral restoration, basically asymptotic freedom, and is not well understood. Thus, what we outline should be considered as tentative.

Based on [4] (which is certainly viewed in the community as controversial), for  $\rho = 3\rho_0$  we are slightly beyond the critical density  $\rho_c$  for chiral restoration. This means that in the chiral limit (bare quark masses zero) the nucleon effective mass is zero. Thus, nucleons behave as massless particles, interact via vector potentials. In any case, nucleon flow in heavy ion collisions is determined chiefly by the vector interactions. From the flow we can try to deduce the magnitude of these interactions, in particular, from Au+Au collisions at 1 GeV/nucleon carried out at GSI [8]. Two groups [9,10] have been working to deduce the vector mean field from the data. This is not simple to do, because the heavy-ion collisions are very nonequilibrium and large explicitly momentum-dependent corrections must be made before one deduce the vector mean field. Still, the two groups are in general agreement. The more complete work of Sahu and Cassing [10] places the vector mean field  $\sim 10\%$  below the DBHF one in magnitude at  $\rho \sim 3\rho_0$ , namely  $V = 460$  MeV at this density. That of [9] places it slightly above the DBHF value. Note that this DBHF value is arrived at by standard rescattering corrections to the mean field extrapolated linearly from  $\rho = \rho_0$ .

Empirically, as can be seen in Figure 2, the flow in Au+Au collisions is already decreasing by the time  $E_{beam}/A = 1$  GeV. At this energy the transport calculation show that the density  $\rho \sim 3\rho_0$  is reached. Higher densities are reached at higher bombarding energies.

From the figure it is clearly seen that the flow decreases rather strongly above  $E = 1$  GeV/N. Sahu and Cassing model this decrease by a vector mean field which goes to zero at higher densities.

Since, in the transport calculation [9,10], densities of  $\rho \sim 3\rho_0$  are reached for Au+Au at 1 GeV/N and since, according to [4], chiral restoration has already occurred by this density, we interpret the decrease in vector mean field with increasing density as a manifestation of asymptotic freedom. Indeed, from lattice calculations of the quark number susceptibility, at zero baryon chemical potential, it is seen that the effective vector coupling decreases by an order of magnitude – but does not go to zero – in going through the

phase transition [12]. In this reference it is made clear that the (Fierz) colored gluon exchange takes over from the  $\omega$ -meson exchange as the temperature goes up through the phase transition. Thus, we have an effective vector mean field remaining above  $T_c$ . One would expect the same general behavior with density, except that the decrease in vector mean field does not seem to be so rapid with density as with temperature.

Given the behavior of the vector mean field described above, we feel that the most favorable density for hyperons in nuclei is  $\rho \sim 3\rho_0$ . As asymptotic freedom sets in at higher densities, the situation will become less favorable.

## 2. NUCLEON-HYPERON INTERACTION

In discussing interactions between the nucleon and hyperons, those from the exchange of vector particles should be straightforward. Beginning with the vector dominance of Gell-Mann, Sharp and Wagner [13] and continuing through the theories in which vector mesons are viewed as gauge particles of hidden symmetries [14], the  $\omega$ -meson is coupled to the baryon number in nonstrange quarks, and the  $\rho$ -meson by SU(3) symmetry, simply related to the  $\omega$ -coupling ( $9g_{\rho NN}^2 = g_{\omega NN}^2$ ).

In the case of the scalar  $\sigma$ -meson, the situation is more complicated. The scalar attraction which binds nuclei results from an enhancement, through scalar interactions, of two-pion exchange, the two pions being correlated in a relative S-state. For nucleon-hyperon interactions, correlated  $K\bar{K}$  states also enter, becoming relatively more important as the strangeness of the hyperon increases. The correlated  $\pi\pi$  or  $K\bar{K}$  interactions are shown in Figure 3.

The scalar interactions have been calculated for many years now in the case of the nucleon-nucleon potential, and are well understood. Recently, the calculation of the nucleon-hyperon interaction by boson exchange has been taken up by the Jülich group [15]. Coupling constants of the  $\pi$  and  $K$  to nucleons and hyperons are determined by SU(3) symmetry. Energy denominators etc. are taken empirically and involve a lot of SU(3) symmetry breaking, arising chiefly from the relatively large strange quark mass  $m_s \sim 150$  MeV, which results in the large kaon mass  $m_K \simeq 495$  MeV. The large kaon mass means that kaon exchange is somewhat suppressed with respect to pion exchange, so there is no simple rule, as in the case of vector meson exchange, for obtaining the couplings of the effective  $\sigma$  by quark counting. None the less, there is an effective symmetry, which we can discover by removing the explicit symmetry breaking in the meson propagators, the wavy lines in Figure 3.

Let us consider how the kaon mass diminishes the kaon exchange in processes such as shown in Figure 3. The kaon propagator is

$$D_K(q) = \frac{1}{q^2 + m_K^2 - \omega^2}. \quad (3)$$

We neglect recoil, setting  $\omega = 0$ . (Since off-diagonal matrix elements like  $\Lambda + \pi \rightarrow \Sigma$  in intermediate energy states are involved, this may be an even cruder approximation than in the case of the nucleon-nucleon interaction.) Now  $|\vec{q}|$  will be limited by the form factor, which generally has a scale of  $\Lambda \sim 1$  GeV  $\sim 2m_K$ . Thus, the  $m_K^2$  in the denominator of Eq. (3) should be an  $\sim 25\%$  effect. Given that two meson exchanges are involved in the interaction, the explicit chiral symmetry breaking through the presence of the kaon mass

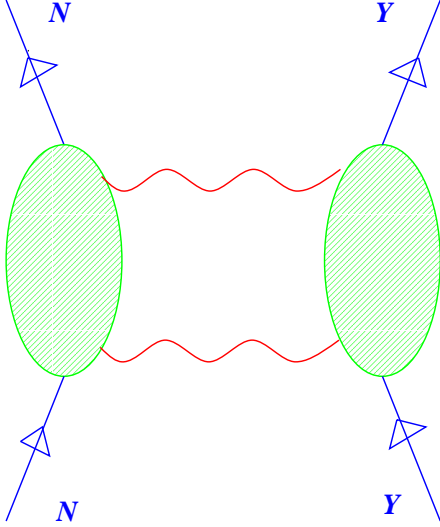


Figure 3. Correlated  $\pi\pi$  or  $K\bar{K}$  interactions, the wavy lines showing the exchanged mesons. The shaded blobs stand for all possible intermediate states.

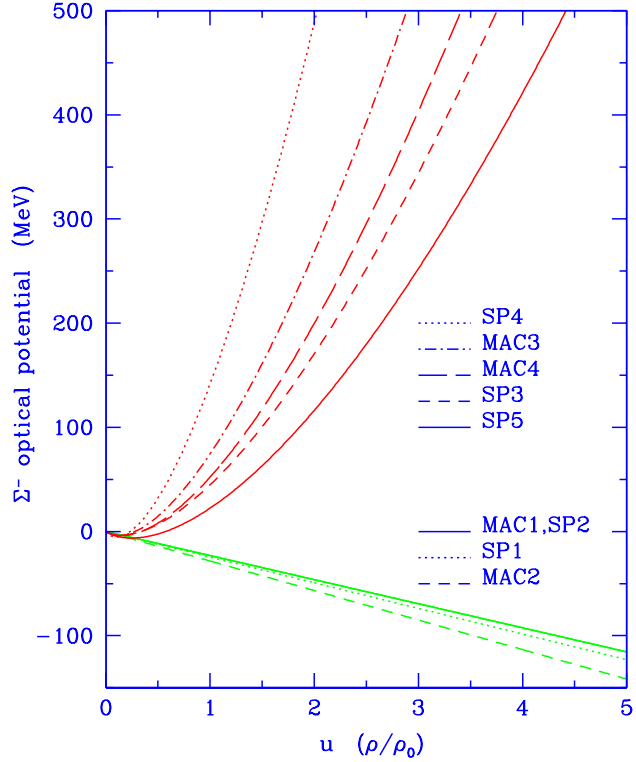


Figure 4.  $\Sigma^-$  optical potentials of [19] in symmetric nuclear matter. Here we used the reduced  $\Sigma^-$ -nucleon mass as free  $\Sigma^-$  mass as mentioned in [21]. For neutron dominant matter,  $\Sigma^-$  feels more repulsion. The upper curves from the density-dependent analyses are favored. The lower curves are for no density dependence, i.e. an optical potential linear in the density.

in the denominators roughly estimated to be an  $\sim 50\%$  effect. Of course there is further chiral symmetry breaking in the “blob” in Figure 3, which we neglect.

The most extensive meson exchange analyses have been performed by Reuber[15]. We show these in Table 1, where the full model calculations are shown, also those from correlated  $K\bar{K}$  exchange. Note that the latter become more important with increasing strangeness, a fact that will turn out to be most important.

In the last row here we have tried to reconstruct what the interactions would be were the kaon mass equal to zero. In fact, with our coupling of the vector interactions to the baryon number in nonstrange quarks, the  $N\Lambda$  coupling shown in Table 1 is unsatisfactory. In order to reproduce the known  $\Lambda$  binding energy in heavy hypernuclei, Ma et al. [16] had to use a ratio of  $g_{\Lambda\Lambda\omega}/g_{NN\omega}$  of 0.512 instead of the 2/3 we propose. If the 2/3 is used, then the  $N\Lambda$  coupling must be increased to  $\geq 0.6$  (In [17] the  $N\Lambda$  coupling is 0.619.) We

Table 1

Effective  $\sigma$  coupling strength for correlated  $\pi\pi$  and  $K\bar{K}$  exchange for various baryon-baryon channels, from [15].

	$NN$	$N\Lambda$	$N\Sigma$	$N\Xi$
Full Model	5.87	2.82	2.58	1.19
( $K\bar{K}$ )	1.00	1.02	1.52	0.84
1.5 ( $K\bar{K}$ )	1.50	1.53	2.28	1.26
Full Model $\star$	6.52	3.33	3.34	1.61

$\star$  Full model with ( $KK$ ) replaced by  $1.5(KK)$ .

do not know the underlying origin of this, but the evidence of this larger  $N\Lambda$  coupling is persuasive. (The  $\Lambda$  binding energies only determine the ratio of  $g_{\Lambda\Lambda\omega}/g_{\Lambda\Lambda\sigma}$  [18]. Thus, phenomenology does not give a clue to whether  $g_{\Lambda\Lambda\sigma}$  is large or small, unless  $g_{\Lambda\Lambda\omega}$  is fixed by theory, or vice versa.)

Our theme is that the explicit symmetry breaking by the kaon mass decreases the  $N\Sigma$  coupling more than the  $N\Lambda$  one, and proportionately decreases the  $N\Xi$  coupling, so that roughly

$$\frac{g_{N\Sigma}}{g_{N\Lambda}} \sim 0.9; \quad \frac{g_{N\Xi}}{g_{N\Sigma}/2} \sim 0.9, \quad (4)$$

certainly valid to within the accuracy of the calculations. (Remember that the interactions go with the square of the coupling constant.) In Figure 4 we show the  $\Sigma^-$ -potential which would be obtained from the parameters in Table 11 of [19]. The repulsive potentials result from the density-dependent optical model potentials which the authors of [19] favor. The density dependent potentials give a strong repulsion at  $\rho \sim 3\rho_0$ . Extrapolation to these high densities may not be warranted. In any case, the repulsions sum to rule out  $\Sigma^-$ -hypernuclei [19]. We suggest, on the basis of our reconstruction of the interaction in the chiral limit that at least some of the difference between  $\Lambda$  and  $\Sigma^-$  couplings derives from the explicit chiral symmetry breaking.

Emulsion data, summarized in [20], showed a consistency for a  $\Xi$ -nucleus potential depth of  $\sim 24$  MeV attraction. This has recently been challenged by KEK quasifree production of the  $\Xi$  in  $^{12}\text{C}$  where it is claimed that the potential, still attractive, is perhaps shallower, down to  $\sim 15$  MeV. In Balberg and Gal [21], the  $\sim 15$  MeV was assumed. With this assumption the cascade particle replaced the  $\Sigma^-$  rather rapidly as a function of density.

The results in Table 1 disfavor the  $\Xi^-$  as compared with the  $\Sigma^-$  in that the attraction is smaller, cut down by a factor  $\sim (0.9)^2$  (See Eq. (4)). The role played by the  $\Xi^-$  is uncertain, since its interaction with nucleons is not pinned down well empirically.

### 3. KAON INTERACTION IN DENSE MATTER AND KAON CONDENSATION

The attraction resulting from the partial restoration of explicit chiral symmetry breaking felt by kaons in nuclear matter was a surprise when first presented by Kaplan and Nelson [22]. It was recently argued by Brown and Rho [23] that at supranuclear densities,

this attractive scalar field could be considered to be the same sort of scalar field we considered in section 2 between nuclear matter and the nonstrange antiquark in the kaon. The difference from hyperonic interaction in dense matter is that for the  $K^-$ -meson, composed of up-antiquark and strange quark, the vector interaction, because of G-parity, gives an attractive interaction on the nonstrange antiquark. Thus, the scalar and vector interactions add in magnitude, both furnishing attraction. Clearly this attraction is expected to be large in magnitude.

Much has been written about  $K^-$ -nuclear matter interactions, and has most recently been summarized in [24]. Important experimental results have recently been published by the KaoS collaboration. In Ni+Ni at 1.8 GeV, densities up to  $\sim 2\rho_0$  are reached. (The precise density depends, of course, on the mean field used in the transport calculations, so even this is somewhat model dependent.) Results for subthreshold  $K^-$ -production are shown in Figure 5. The mean fields used to calculate in-medium effects are shown in Figure 6.

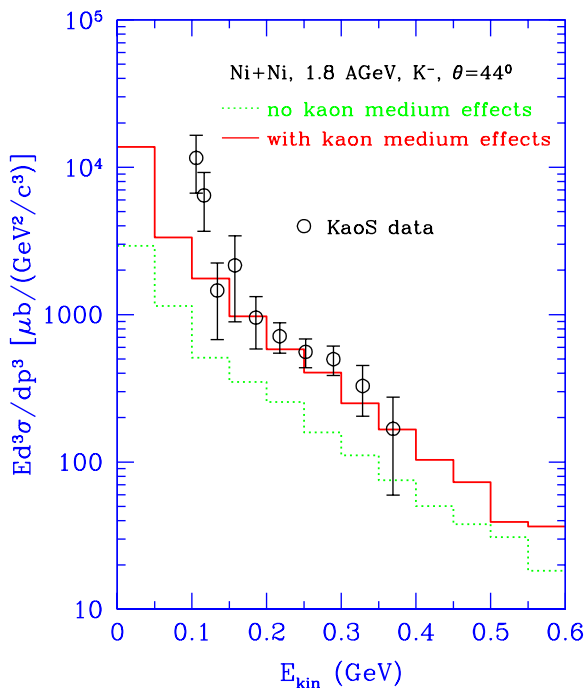


Figure 5.  $K^-$  spectra in Ni+Ni collisions at 1.8 A GeV beam kinetic energy.

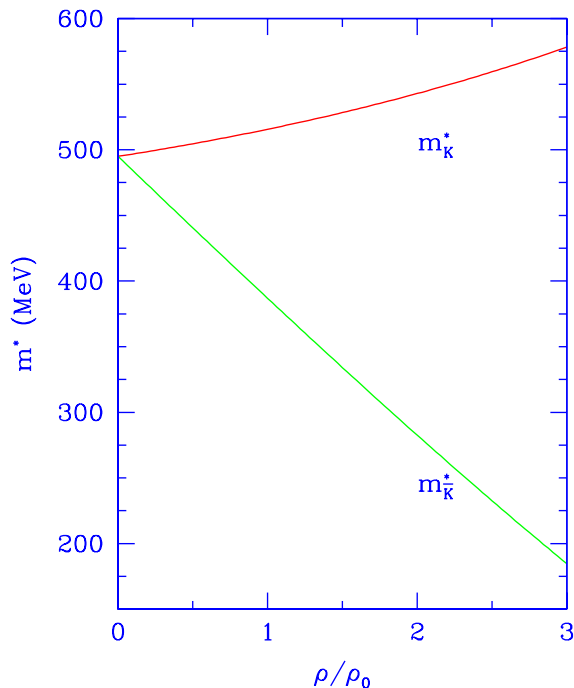


Figure 6. Effective mass of kaon and antikaon in nuclear medium.

There is general agreement between the theoretical groups of [24] and that of Cassing et al. [26] on the fits to the  $K^-$ -spectra. In a footnote in [26] the  $K^-$ -mass drops slightly more rapidly than in our Figure 5 (although uncertainties are emphasized there).

The KaoS experiments are particularly useful in investigation of mean field effects. The  $K^-$ -production would be 235 MeV below threshold for 1.8 A GeV Ni+Ni, whereas a mean field such as produces  $m_{K^-}^*$  shown in our Figure 5 would put the production locally

at threshold at the  $\sim 2\rho_0$  density formed in central collisions. The extrapolation of the curve from  $2\rho_0$  to  $3\rho_0$  is not determined by the present experiments, but will be checked by subthreshold  $K^-$ -production in Au+Au collisions, which do reach  $\rho \sim 3\rho_0$  and which are now going on. Note that the subthreshold kaon production is insensitive to the low densities involved in  $K^-$ -atoms and do not bear on the results of Friedman, Gal and Batty [27].

A dramatic result of medium effects is shown in Figure 7, where the ratio of  $K^+/K^-$  production, each chosen at an energy which would be 235 MeV below threshold in nucleon-nucleon collisions. It is seen that this ratio is changed by an order of magnitude by medium effects. This is because the  $K^+$ -meson experiences scalar and vector mean fields of opposite sign, which tend to cancel each other.

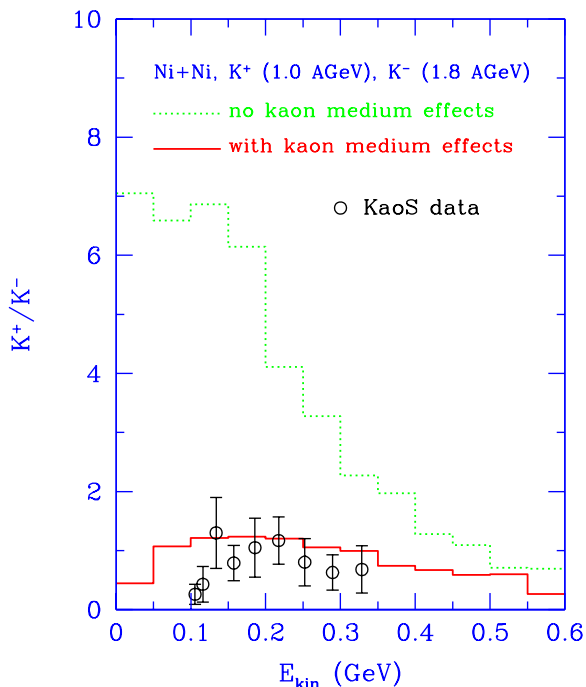


Figure 7. Kinetic energy spectra of  $K^+/K^-$  in Ni+Ni collisions at 1.0 AGeV ( $K^+$ ) and 1.8 AGeV ( $K^-$ ). The solid and dotted histograms are the results with and without kaon medium effects, respectively. The circles are the experimental data from the KaoS collaboration [25].

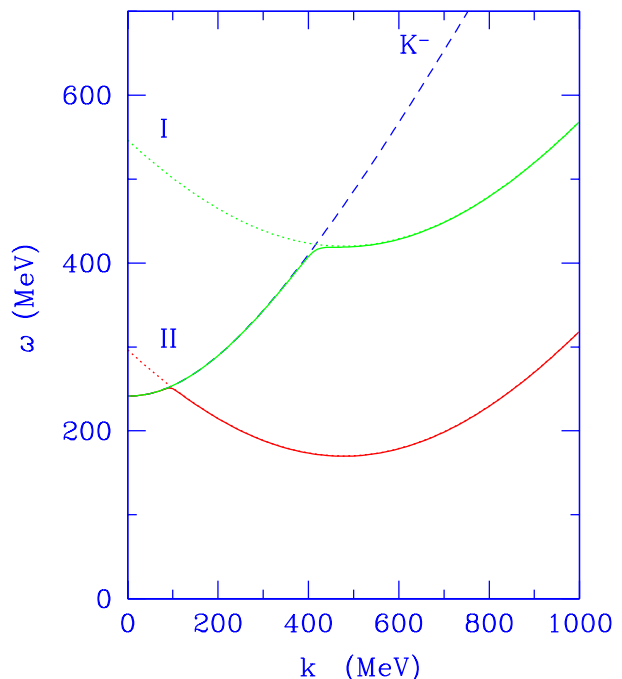


Figure 8. Lowest branches of kaesobar at  $\rho = 3\rho_0$ . Lines I and II represent the lowest  $\Sigma^-$ -particle-neutron-hole branches corresponding to  $V_{\Sigma^-}(3\rho_0) = 250$  MeV, 0 MeV, respectively. The solid lines are the possible lowest kaesobars which follow the minimum energy solution between  $K^-$  and  $\Sigma^-$ -particle-neutron-hole branch.

Now the electron chemical potential  $\mu_e$  is  $\sim 210$  MeV at  $\rho \sim 3\rho_0$  [28]. As soon as the  $K^-$ -mass drops down to  $\mu_e$ , kaons will replace electrons in neutron stars, with many dramatic consequences, as outlined in [28,29].



There have been many articles in the literature, most recently Ref. [30], saying that the introduction of hyperons early in density precludes kaon condensation by lowering the electron chemical potential. Whereas it is clear that the two schemes are somewhat competitive, one should realize that at the temperature involved in stars,  $T \sim 50$  MeV, all normal modes with electron charge will be excited with appropriate Boltzmann factors. The  $K^-$  and  $\Sigma^-$ -neutron hole ( $\Sigma^- N^{-1}$ ) interact, except at momentum  $k = 0$ , and one should diagonalize these excitations in order to find the normal mode, the kaesobar [24]. We show this construction in Figure 8. Lines I and II represent the lowest possible  $\Sigma^-$ -particle-neutron-hole branches corresponding to  $V_{\Sigma^-}(3\rho_0) = 250$  MeV, 0 MeV, respectively. The solid lines are the lowest possible kaesobars which follow the minimum energy solution between  $K^-$  and the  $\Sigma^-$ -particle-neutron-hole branch. Here we used  $\Phi(3\rho_0) = 700$  MeV,  $W(3\rho_0) = 460$  MeV,  $R(3\rho_0) = -51$  MeV,  $x_{\sigma K} = x_{\omega K} = 1/3$ ,  $x_{\rho K} = 1/9$ , and  $x_{\sigma\Sigma} = 0.5$  in the meson exchange model (see Appendix of [24]). In order to specify the  $\Sigma^-$  potential, we used  $x_{\omega\Sigma} = x_{\rho\Sigma} = 1.174, 0.667$  for lines I and II, respectively. (For case I the full mean field potential felt by the  $\Sigma^-$ , vector plus scalar, is 250 MeV. Given the mean fields  $\Phi, W, R$  these  $x_{\omega\Sigma}$  and  $x_{\rho\Sigma}$  are what we needed to reproduce the two curves.) The value  $V_{\Sigma^-}(3\rho_0) = 250$  MeV for curve I is taken from the least repulsive of the upper curves of Figure 4. Curve II lies much lower, since we used 2/3 of the reduced vector field of  $W = 460$  MeV on the nucleon but 1/2 of the very large (attractive) 700 MeV scalar potential on the nucleon which is typical of Walecka mean field theories. Although curve II lies much lower than curve I, we believe that such a scenario might result from theories which have the strong scalar attraction of Walecka-like theories.

In the sense that the upper curve in Figure 8 follows from the least repulsive mean field in the extrapolation of empirical data [19], one might think that the  $\Sigma^-$  does not enter in dense matter. However, scalar mean fields of the size we employed in case II are needed for chiral restoration at  $\rho \leq 3\rho_0$ . Furthermore we have argued that the vector mean fields are substantially reduced from those of the linear Walecka model. We offer case II as a model which roughly incorporates this features.

## REFERENCES

1. G. Baym and S.A. Chin, Phys. Lett. 62B (1976) 241.
2. G. Choplive and M. Nauenberg, Phys. Rev. D16 (1977) 450.
3. H.A. Bethe, G.E. Brown and J. Cooperstein, Nucl. Phys. A462 (1987) 791.
4. G.E. Brown, M. Buballa and Mannque Rho, Nucl. Phys. A609 (1996) 519.
5. G.Q. Li and G.E. Brown, to be published.
6. B.D. Serot and J.D. Walecka, Adv. Nucl. Phys. 16 (1986) 1.
7. R. Brockmann and H. Toki, Phys. Rev. Lett. 68 (1992) 3408.
8. N. Hermann, FOPI collaboration, Nucl. Phys. A610 (1996) 49c.
9. G.Q. Li, G.E. Brown, C.-H. Lee and C.M. Ko, work in progress.
10. P.K. Sahu and W. Cassing, work in progress.
11. W. Reisdorf and H.G. Ritter, Ann. Rev. Nucl. Part. Sci., to appear Dec. 1997.
12. G.E. Brown and Mannque Rho, Phys. Repts. 269 (1996) 334.
13. M. Gell-Mann, D. Sharp and W.G. Wagner, Phys. Rev. Lett 8 (1962) 261.

14. M. Bando, T. Kugo and K. Yamawaki, Phys. Repts. 164 (1988) 217.
15. A. Reuber, K. Holinde, H.-C. Kim and J. Speth, Nucl. Phys. A608 (1996) 243.
16. Z.-Y. Ma, J. Speth, S. Krewald, B. Chess and A. Reuber, Nucl. Phys. A608 (1996) 305.
17. J. Mareš and B.K. Jennings, Phys.Rev. C49 (1994) 2472.
18. N.K. Glendenning and S.A. Moszkowski, Phys. Rev. Lett. 67 (1991) 2414.
19. C.J. Batty, E.Friedman and A. Gal, Phys. Rept. 287 (1997) 385.
20. C.B. Dover and A. Gal, Ann. Phys. 146 (1983) 309.
21. S. Balberg and A. Gal, Nucl. Phys. A 625 (Dover Memorial Volume, 1997) 435.
22. D.B. Kaplan and A.E. Nelson, Phys. Lett. B 175 (1986) 57; A.E. Nelson and D.B. Kaplan, Phys. Lett. B192 (1987) 193.
23. G.E. Brown and Mannque Rho, Nucl. Phys. A596 (1996) 503.
24. G.Q. Li, C.-H. Lee and G.E. Brown, Phys. Rev. Lett, in press; Nucl. Phys. A 625 (Dover Memorial Volume, 1997) 372.
25. R. Barth and the KaoS Collaboration, Phys. Rev. Lett. 78 (1997) 4027; P. Senger for the KaoS Collaboration, Heavy Ion Physics 4 (1996) 317; P. Senger for the KaoS Collaboration, Acta. Physica Polonica B27 (1996) 2993.
26. W. Cassing et al., Nucl. Phys. A614 (1997) 415.
27. E. Friedman, A. Gal and C.J. Batty, Phys. Lett. B 308 (1993) 6; Nucl. Phys. A579 (1994) 578.
28. V. Thorsson, M. Prakash and J.M. Lattimer, Nucl. Phys. A 572 (1994) 693.
29. G.E. Brown and H.A. Bethe, Ap.J. 423 (1994) 659.
30. J. Schaffner and I.N. Mishustin, Phys. Rev. C53 (1996) 1416.